

Summary of the fundamental plasma physics session in the 1st AAPPS-DPP conference

M. Xu^{1*}, G.Z. Hao¹, P.H. Diamond^{2,1},

¹*Southwestern Institute of Physics, Chengdu 610041, China*

²*University of California at San Diego, La Jolla, California 92093, USA*

Abstract

Understanding of fundamental plasma physics contributes to progress in plasma science in many fields, such as magnetic confinement fusion, solar/space physics and application of plasma techniques. Intersecting common fundamental problems stimulate cross-fertilization of different topical areas. This paper summarizes highlights of progress reported in the Fundamental Plasma Physics Session of the 1st conference of Association of Asia Pacific Physical Societies-Division of plasma physics (AAPPS-DPP). Progress in the following fields is reviewed: (i) basic plasma theory; (ii) self-organization; (iii) reconnection and particle acceleration; (iv) magneto-hydrodynamics (MHD) instabilities and energetic particle physics; (v) magnetic confinement physics fundamentals; and (vi) exploiting fundamentals for performance.

I. INTRODUCTION

Understanding of fundamental plasma physics is essential for progress in many areas (fig. 1), such as the magnetic confinement fusion energy (MFE), laser acceleration, inertial confinement fusion(ICF), space/solar physics, and for the development of plasma technique applications. Fundamentals are related to and supply potential resolutions for key problems in various plasma physics areas. Examples of such key problems include the drift wave turbulence and associated transport in MFE, mechanism of accelerating and heating particles in laser plasma, characteristics of strongly correlated systems in basic plasma field, plasma material interaction in applied areas, mechanism of magnetic reconnection in solar and astro-physics, and particle acceleration in space physics. Fundamental problems stimulate cross-fertilization of different topical areas. Fundamentals are the base of, and support for the progress in various plasma physics areas.

This paper summarizes the presentations, which were reported in the Fundamental Plasma Physics Sessions of the 1st conference of AAPPS-DPP¹. The sessions include 4 plenary, 26 invited, 10 oral and 1 poster presentations, of which the inventory is shown in table 1. Highlights of progress in the following topics are presented in this paper: (i) basic plasma theory; (ii) self-organization; (iii) reconnection and particle acceleration; (iv) magneto-hydrodynamics (MHD) instabilities and energetic particle physics; (v) magnetic confinement physics fundamentals; and (vi) fundamentals for performance.

Topics		Presenters
Basic plasma theory		T. Chiueh, S.H. Chen, P. H. Diamond, D. Escande, D. Guo, Z.B. Guo, T. Watanabe
Self-organization	a) Flows	S.Inagaki, T. Long, T.T. Tran, G. Tynan, L. Wang, K. J. Zhao
	b) Magnetic	J. Cho, R. L. Dewar, M. Veranda
Reconnection & particle acceleration		F. Guo, M. Hirota, Y.H. Liu, Z.W. Ma, R.Numata, H. Tanabe, G. Vekstein, Y. Wan
MHD & Energetic particle physics		M. Furukawa, D. Li, R.R. Ma, S.S. Seo, S. D. Song
Magnetic confinement physics fundamentals		H.T Chen, M.K. Han, R. Ke, J. Liu, H. Sugama, Z.B. Shi, Y. Tian, M.G. Yoo, B.Y. Zhang
Exploiting fundamentals for performance		Z.H. Wang

Table 1: Inventory of the presentations.

In section II, the results on the dynamics of binary fluid system and a theory about basic plasma phenomena are discussed. The elastic waves are found to play an important role

Fundamentals are central for plasma physics

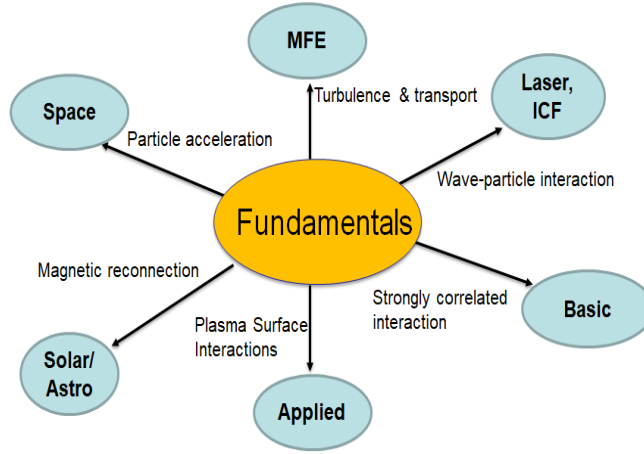


FIG. 1: Fundamentals are central for various plasma physics areas.

in defining a length for the larger blob structures. In section III, the progress of the flows generated by turbulence, effect of shear flow on turbulence and their cross-interaction are addressed. A new self-organized magnetic state is theoretically predicted and experimentally confirmed, in reversed-field pinch configuration. There, the formation of barriers to the wandering of magnetic field lines is observed. In section IV, the new theory models and experiments about magnetic reconnection and particle accelerations are introduced. It is demonstrated that the force balances in inflow and outflow direction, respectively, determine magnetic reconnection rate. The heated electrons are localized in the region near the X-point. The heated ions are distributed in the outflow regions. Section V reports the progress on the MHD instabilities and energetic particle physics in toroidal plasma. The anti-Hermitian contributions, due to wave-energetic particle resonance, can twist the radial mode structure, and lead to up-down asymmetry in the global mode structure. Section VI shows the new results on the fundamentals of magnetic confinement physics. In Ohmic breakdown, the self-electric field results in significant decrease of avalanche growth rate which leads to relatively slow plasma formation. Section VII introduces a newly developed module for the BOUT++ framework for studying interaction between neutral gas and plasmas. Conclusions are drawn in the last section.

II. BASIC PLASMA THEORY

Basic plasma theory was established for fundamental research of the systems with collective electromagnetic interactions. In this section, we mainly report progress of some basic plasma theories, such as the turbulence, Debye shielding and Landau damping. The experimental study of Reynolds stress associated with turbulence is also mentioned, which supplies a potential topic for turbulence theory research.

Diamond presented a theoretical model for 2D Cahn-Hilliard-Navier-Stokes(CHNS) turbulence, which can be applied to investigate the spinodal decomposition process of a binary liquid mixture accompanied by temperature quench. The 2D CHNS system is analogous to 2D magnetic-hydrodynamics (MHD) system. Hence, they have some similar features: (i) The surface tension force in the CHNS system is similar to $\mathbf{J} \times \mathbf{B}$ force in the MHD system. Here, \mathbf{J} is current, and \mathbf{B} is magnetic field. (ii) The ideal quadratic conserved quantities have the similar form, which leads to the similar cascade directions in these two systems. (iii) The dispersion relation of linear elastic wave in the CHNS system is similar to Alfvén wave in the MHD system^{2,3}. However, the kinetic energy spectrum in the CHNS system is different from that in the MHD system. The basic equations for describing the 2D CHNS system can be found in Ref. 2.

The developed CHNS theory reveals the important role of elastic waves in the dynamics of the CHNS turbulence. In the elastic region, the $-7/3$ power law of mean square concentration spectrum $H_k^\psi \sim k^{-7/3}$ (Fig. 2) is robust. The elastic range depends on relative scale between the Hinze scale(L_H) and dissipation scale L_d . At the Hinze scale, kinetic and elastic energies balance. When $L_H \gg L_d$, the elastic range is relatively longer in k (wave number) space and the elastic restoring force (due to the surface tension) works on the CHNS system. The smaller external force intensity (i.e. smaller $f_{0\phi}$ in Fig. 2) results in larger L_H . Hence, the elastic range becomes larger at smaller $f_{0\phi}$. This enhances the inverse cascade process of $\langle \psi^2 \rangle_k$, which generates the large scale blob structure as shown in the upper panels in Fig. 3. For comparison, a case with shorter elastic range is shown in the bottom panels in Fig. 3. The blob growth is arrested there.

The 2D CHNS theory model is applied to study time evolution of the concentration field ψ in the background of a single eddy. It is shown that the evolution of ψ passes three stages: (A) formation of a "jelly roll" pattern, (B) a change in topology, and (C)

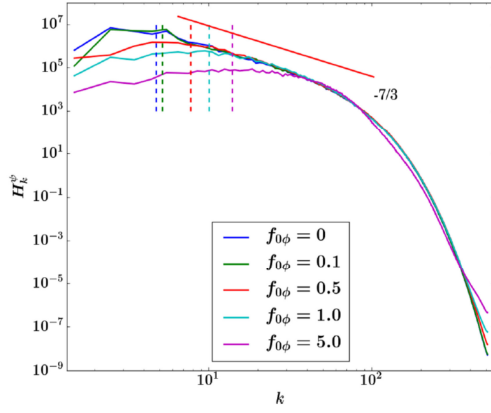


FIG. 2: Power law of the mean square concentration spectrum H_k^ψ for difference intensities of the external force $f_{0\phi}$. Reproduced with permission from [2].

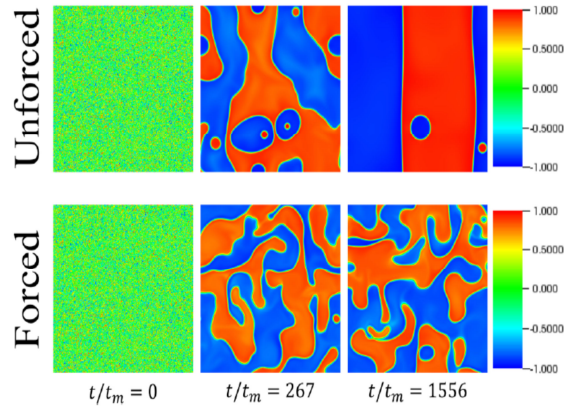


FIG. 3: Top panels are plots of the ψ field (for the unforced case) at different times. Note that phase separation is nearly complete in this case. Bottom panels are ones for the forced case². Here, fluid shearing creates finite sized concentration blobs in a finite time.

Reproduced with permission from [2].

formation of a target pattern. The target pattern is metastable, and the rings merge with each other on a time scale exponentially long relative to the eddy turnover time. The merger occurrences are associated with dips in the elastic energy evolution³. The merger process has same similarities to the drift-Zonal-Flow(ZF) staircases in the magnetic confined plasma turbulence.

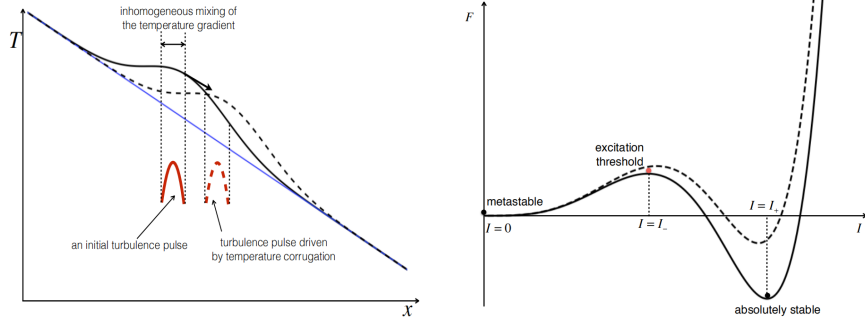


FIG. 4: Sketch of the temperature corrugations (left) and the final, absolutely stable state formed by corrugation front propagation (right).

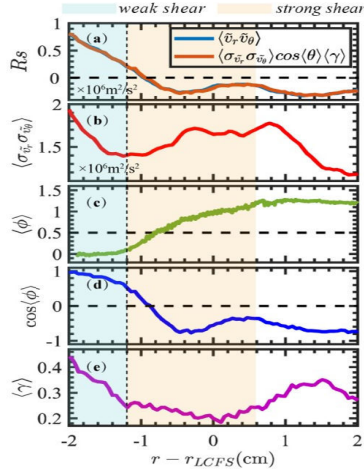


FIG. 5: In the edge region of HL-2A tokamak plasma, the spatial profile of the Reynolds stress (a), fluctuation intensity (b), cross phase (c and d) and coherence (e). Reproduced with permission from [4].

Z.B. Guo's presentation showed that the inhomogeneous mixing of turbulence corrugates the mean temperature profile, and the temperature corrugation then induces the sub-critical bifurcation of turbulence. Consequently, the system will make a transition from a metastable laminar state to an absolutely stable, excited state (Fig.4). Incorporating spatial coupling of the locally excited turbulent regions, a front forms. This front connects the excited and laminar states and efficiently penetrates the linear stable region. This bi-stable turbulence spreading can explain observations of hysteresis in the intensity of L-mode core turbulence in tokamak plasma.

D. Guo studied the dependence of Reynolds stress on the cross phase of fluctuations, based

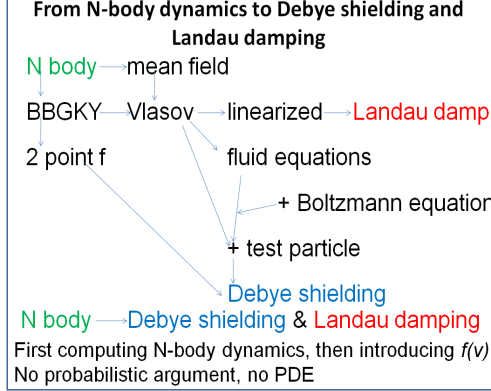


FIG. 6: Sketch: from N-body dynamics to the Debye shielding and Landau damping.

on the experimental measurements. It is well known that the Reynolds stress is related to the velocity fluctuations, $\mathbf{\Pi}^{Ref} \sim \langle \tilde{v}_r \tilde{v}_\theta \rangle = \langle \sigma_{\tilde{v}_r} \sigma_{\tilde{v}_\theta} \rangle \cdot \cos\langle\phi\rangle \cdot \langle\gamma\rangle$. In recent experiment on the HL-2A tokamak, it is observed that in the region with strongly shear rotation, the coherence $\langle\gamma\rangle$ and the fluctuation intensity $\langle \sigma_{\tilde{v}_r} \sigma_{\tilde{v}_\theta} \rangle$ vary slightly, whilst the Reynolds stress varies directly with cross phase $\cos\langle\phi\rangle$. In the weaker shear region, $\mathbf{\Pi}^{Res}$ increases with $\langle\gamma\rangle$ and $\langle \sigma_{\tilde{v}_r} \sigma_{\tilde{v}_\theta} \rangle$, as shown in Fig. 5. These indicate that, in the strongly shear region, the cross phase has a dominant contribution to Reynolds stress. However, in the weak shear region, the coherence and fluctuation are dominant⁴. In addition, Long reported the measurement results of the poloidal residual stress, which is a part of Reynolds stress. The results suggest that a poloidal intrinsic torque exists at the plasma boundary, and its radial gradient can serve as an intrinsic torque to generate a net velocity shift with respect to the neoclassical poloidal velocity.

Escande showed that the basic phenomena, such as the Debye shielding and Landau damping, can be directly derived through the use of N-body mechanics with the Newton's second law^{5,6} and standard tools of calculus. The new derivations bring more insights on basic plasma theory, such as creating a connection between Debye shielding and Landau damping. It is found that each particle has two contributions to potential: a short-range one and long-range one. The short-range one results in Debye shielding. Debye shielding and collisional transport are two sides of the same coin: repulsive deflections. The long-range one leads to two phenomena: excitation of the Langmuir wave and so-called 'Landau damping'^{5,6}.

Self-organization: A Global Perspective

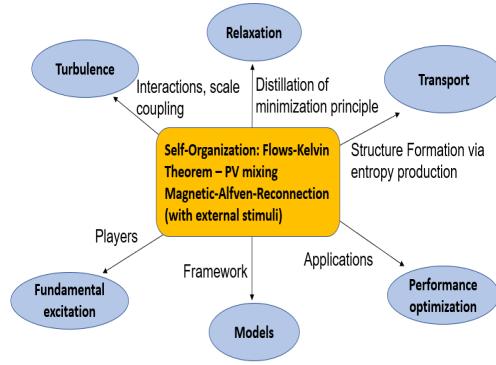


FIG. 7: A global perspective of self-organization.

III. SELF-ORGANIZATION

Self-organization phenomena commonly exist in various systems in nature. Self-organization plays an important role in various topics in magnetized plasma. For example, self-organization is relevant to structure formation via entropy production in transport, distillation of the constrained minimization principle for relaxation of the magnetic field, scale coupling in turbulence, and so on as shown in Fig.7. This section reports the progress of self-organization research related to the flow generation and magnetic field relaxation.

A. Flows

Turbulence induces shear flows without external momentum input in toroidal plasma. The turbulence driven flows are thought to play a key role in (a) L-mode critical gradient confinement⁷; (b) intrinsic rotation⁸; (c) Low to High mode transition in tokamak⁹; (d) origin of density limit¹⁰. The Turbulent structures or associated eddies are tilted and stretched by shear flow. Symmetry breaking induced by tilted turbulent structure reinforces the shear flow. Non-linear interaction between the turbulence and the flow generated by turbulence is an active research topic. In this section, we report the recent progress of the non-linear interaction between turbulence and flow, and of the associated topics in both experiment and theory.

Tynan reported an overview of the study of cross-interaction between turbulence and flows in the linear helicon device-CSDX¹². It was found that the increase of magnetic

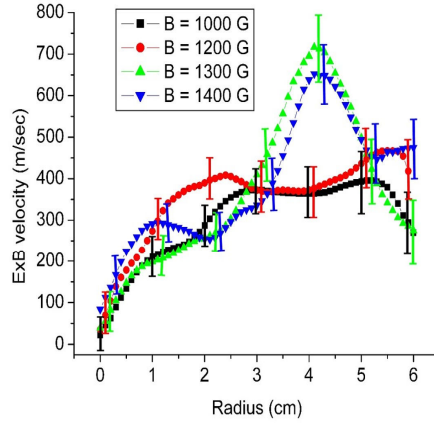


FIG. 8: The measured azimuthal flow (i.e. $\mathbf{E} \times \mathbf{B}$) flow for the cases with different magnetic field \mathbf{B} . The flow shape in the region (radius > 3 cm) has a transition as varying magnetic field. Reproduced with permission from [11].

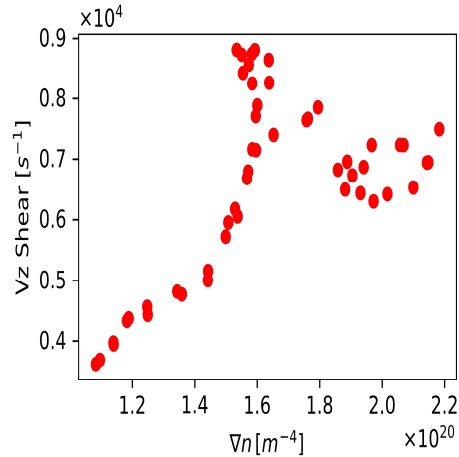


FIG. 9: The measured flow shear as function of the density gradient.

field produces the increase of the core ion temperature and the associated strong radial ion temperature gradient in CSDX. Furthermore, the larger magnetic field leads to the larger azimuthal flows at the edge, and the stronger radially shear flows, as shown in Fig. 8. It is identified that the increases of both temperature gradient in the core and the radially shear azimuthal velocities at the edge are regulated by the drift wave instabilities which appear as the magnetic field strength exceeds a critical value¹¹.

Furthermore, it is shown that a drift wave-zonal flow system reached a self-regulated state by the combination of the particle and vorticity transport¹³. Figure 9 shows that

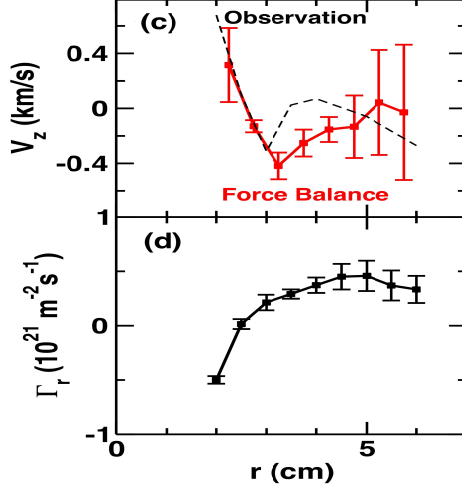


FIG. 10: The radial profile of the axial velocity (a) and particle flux (b). In (a), the dashed and dotted-solid curves are the experimental and force balance model predicted values, respectively¹⁵.

the self-saturation state is reached when density gradient is sufficiently large (i.e. $\nabla n > 1.6 \times 10^{20} \text{ m}^{-4}$)¹⁰. The measurements on the CSDX suggest that turbulence does work on the shear parallel flow (intrinsic flow), which is driven by the residual stress¹⁰. It is also demonstrated that the residual stress is proportional to density gradient, which is consistent with the theoretical prediction¹⁴.

Inagaki examined the flows driven by turbulence in the linear device-PANTA¹⁵ as shown in Fig. 10. The outward particle flux in the region ($r > 2.5 \text{ cm}$) is induced by the drift-waves destabilized by density gradient. The outward transport relaxes the density gradient. On the other hand, inward particle flux at $r=2 \text{ cm}$ is generated by D'Angelo mode instability which is driven by axial flow shear. The inward particle transport steepens the density gradient in the core region. In combination with the generation of shear flow by drift-waves, a cross-interaction structure is formed, by the cross-interaction between different fields (density and velocity) and the corresponding fluxes (particle and momentum), as shown in Fig. 11.

An electromagnetic extended theory of turbulence acceleration was presented by Wang,¹⁶ who received the 2017 DPP Young Researcher Award. The mean flow equation averaged over the flux surface is extended to include the contribution from the electromagnetic ion-temperature-gradient(ITG) turbulence, as presented below.

mode	Drift wave	D'Angelo mode
Driving	∇n	∇V_z
Destabilizing mechanism	Phase shift (in this work electron collision)	'Negative Compressibility' $k_z k_\theta \frac{\partial}{\partial r} V_z > 0$
Transport	Outward particle flux Residual Stress	Inward component in particle flux eddy viscosity on flow

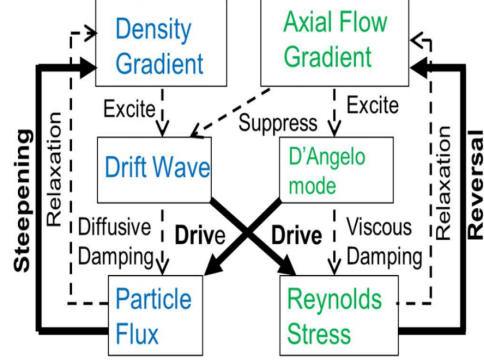


FIG. 11: (left) comparison between D' Angelo mode and drift wave; (right) cross-interaction between the different fields (density and velocity) and corresponding flux (particle and momentum transport)

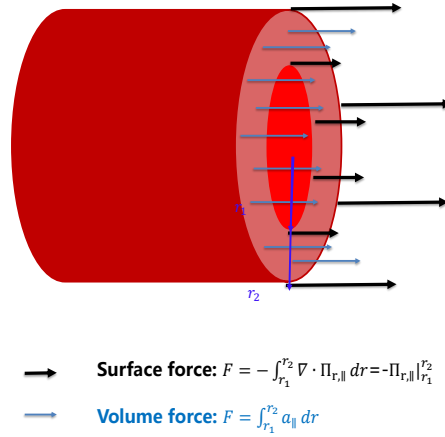


FIG. 12: Sketch of the turbulence acceleration by a volume force a_{\parallel} .

$$\frac{\partial \langle U_{\parallel} \rangle}{\partial t} + \nabla \cdot \Pi_{r,\parallel} = a_{\parallel} \quad (1)$$

Here, $\langle U_{\parallel} \rangle$ denotes the ion flow average over the flux surface, $\Pi_{r,\parallel}$ includes the Reynolds stress Π^{Rey} , kinetic stress and cross Maxwell stress. Here, $a_{\parallel} = a_P + a_M$ is the turbulent acceleration. a_P represents the electrostatic ITG turbulence contribution¹⁶, a_M denotes the driven term related to the ion pressure gradient along the radial magnetic perturbation¹⁷, which is a electromagnetic turbulent acceleration term. $-\int_{r_1}^{r_2} \nabla \cdot \Pi_{r,\parallel} dr$ is a kind of surface force acting on a fluid element, while a_{\parallel} is a volume force which can locally accelerate/decelerate the fluid elements as shown by a sketch(Fig. 12). It is pointed out that

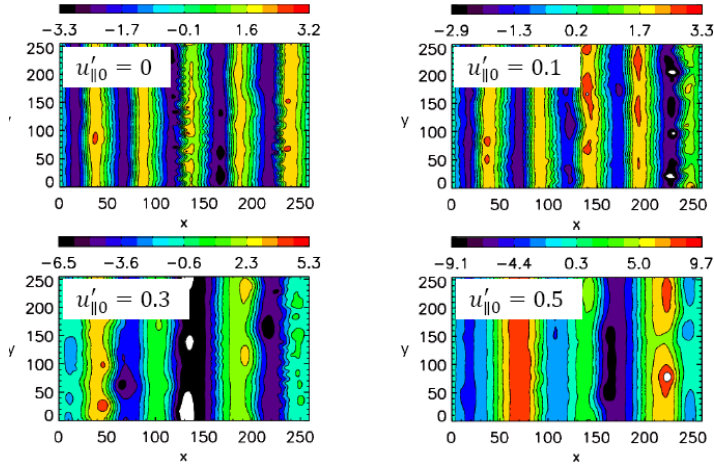


FIG. 13: Zonal-flow structure for the different choices of equilibrium flow shear $u'_{||0}$.

Eq.(1) is derived on the basis of the gyro-kinetic theory¹⁷ and is not in contradiction to the momentum conservation¹⁶.

Tran investigated the role of parallel flow shear in zonal flow (ZF) pattern formation, based on the 3D Hasegawa-Mima equation coupled with ion parallel flow dynamics. In the model, the coupling term includes vortex stretching-like and energy transfer rate terms¹⁸. It is found that the parallel flow shear $u'_{||0}$ enhances the amplitude of ZF and induces the decrease of radial wave number of ZF (Fig.13). The analysis of coupling dynamics shows that the vortex stretching-like term plays a significant role in the ZF enhancement. This is in contrast to the neutral fluid turbulence where it hinders the inverse cascade process. Here, ZF is initially generated by drift wave turbulence at $u'_{||0} = 0$. Furthermore, the confinement is not strongly improved when finite $u'_{||0}$ exists.

Zhao presented the results of synchronization of geodesic acoustic modes (GAMs) and magnetic fluctuations, which was observed in the edge plasmas of the HL-2A tokamak, using multiple Langmuir probe arrays. The temporal evolutions of the Meso-scale Electric Fluctuations (MSEFs) and magnetic fluctuations clearly show the frequency entrainment and phase lock between the GAM and $m/n=6/2$ magnetic fluctuations (Fig.14). Here, m and n are the poloidal and toroidal harmonic number of the perturbations, respectively. The results indicate that the GAMs and magnetic fluctuations can transfer energy through non-linear synchronization. Such non-linear synchronization may also contribute to the low-frequency

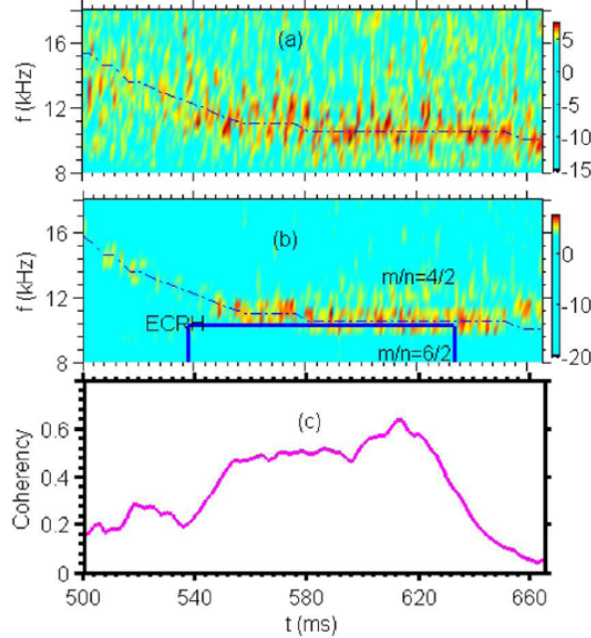


FIG. 14: Spectrograms of the mesoscale electric fluctuations (MSEFs) (a) and magnetic fluctuations of $m/n=6/2$ (b) (the dash-dotted line indicates evolution of the center of the fluctuation frequency). (c) The coherence between the MSEF and magnetic fluctuations.

Reproduced with permission from [19]

zonal flow formation, to the reduction of turbulence levels, and thus affect confinement regime transitions. This is a discovery of an essential structure formations of plasmas, in which the two fundamental vector fields (magnetic field and flow field) dynamically couple together¹⁹.

B. Magnetic

Veranda showed a new self-organized helical Magnetic state in the reversed-field pinch (RFP) configuration (Fig. 15(a)) by 3D nonlinear visco-resistive MHD modelling²⁰ and confirmed by the experiment on the RFX-mod in Padua, Italy. The new helical state, with a twist of a non-resonant MHD mode, was stimulated by the use of small external non-resonant magnetic perturbation (MP) with $(m/n=1/-6)$, which implies there is no corresponding rational surface in the plasma (Fig. 15(b)). Here, m and n are the poloidal and toroidal harmonic number of the MP, respectively. The seed external magnetic field from non-resonant MP imposes its helical pinch to the whole plasma column, and leads to a new

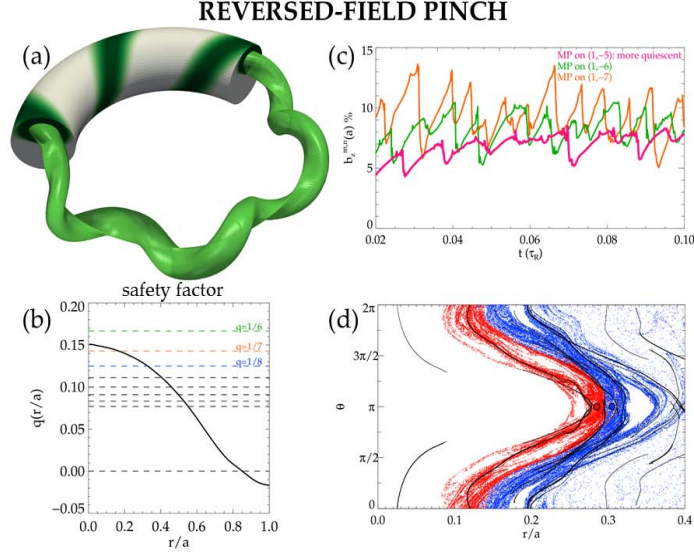


FIG. 15: (a) Cartoon of the Reversed–field pinch (RFP); (b) the typical safety profile of RFP²⁰; (c) temporal dynamics of the magnetic field associated with the dominant MHD mode in different helical states: non resonant states are more quiescent; (d) shows how the field lines, initiated by the colored dots, do not leak (for a finite time) through the Lagrangian Coherent Structures computed in helical states (black curves).

helical state, which is more quiescent compared to the resonant cases, as shown in Fig. 15(c). In addition, Lagrangian Coherent Structures are computed in the weakly stochastic region surrounding the helical core. They are shown to act as barriers to the wandering of magnetic field lines, and possibly make a relevant contribution to the presence of the internal transport Barriers (ITB) in magnetic confinement fusion devices.

Dewar reported the progress of a hydromagnetic dynamical model^{21,22}, Multi-region Relaxed Magnetohydrodynamics (MRxMHD), which has been proposed as a dynamical generalization of Taylor relaxation theory appropriate to toroidally confined plasmas. The core ideal of MRxMHD is to fix MHD by removing the bad constraints (e.g. no heat transport along field line and no magnetic reconnection), but keeping a minimal set of robust ones. In the MRxMHD model, the plasma-magnetic field system as consisting of arbitrarily many regions, each containing compressible Euler fluid and Taylor-relaxed magnetic field, separated by interfaces in the form of flexible ideal-MHD current sheets. Internal self-consistency is guaranteed by deriving its evolution equations from Hamilton's Principle of Stationary

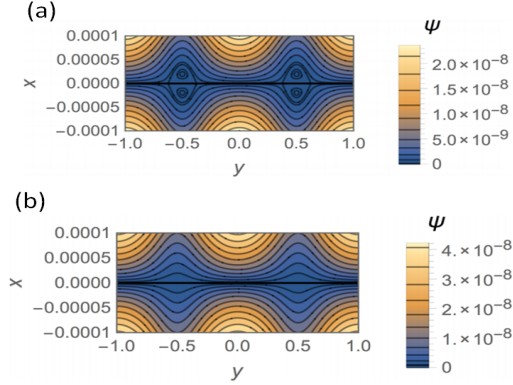


FIG. 16: Level surface of ψ (magnetic surfaces) for cases of ripple amplitude (a) smaller and (b) larger than a threshold. Here, 'x' and 'y' denote the interested relaxed-MHD regions. Horizontal line (i.e. equilibrium current sheet) separates the the upper and lower relaxed-MHD regions. Reproduced with permission from [22].

Action, using the MHD Lagrangian but replacing the local, microscopic constraints of ideal MHD, which freeze in magnetic flux and entropy, with invariance of macroscopic entropy and magnetic helicity integrals over each relaxation region, enforced using Lagrange multipliers. The magnetic field is force-free in each region, it is coupled to the plasma only at the interfaces between the regions. The formalism has flexibility in matching any given pressure and current profile as each region has different temperature and current factor.

The adiabatic limit of MRxMHD is illustrated using a sheared-magnetic-field slab model with rippled radial boundaries and a single plane interface carrying a resonantly excited current sheet²². The adiabatic switching on of boundary ripple excites a shielding current sheet opposing reconnection at a resonant surface (Fig. 16(a)). The perturbed magnetic field as a function of ripple amplitude is calculated by invoking conservation of magnetic helicity in the two regions separated by the current sheet on the interface between two relaxation regions. At low ripple amplitude half islands appear on each side of the current sheet, locking the rotational transform at the resonant value. Above a critical amplitude these islands disappear (Fig. 16(b)) and the rotational transform develops a discontinuity across the current sheet ²². Dynamical MRxMHD model predicted the existence of a threshold Resonant Magnetic Perturbation (RMP) amplitude at which rotational transform jumps across the resonantly excited current sheets occur. This theoretical basis can be used to reconstruct equilibria for tokamak when RMP is switched on.

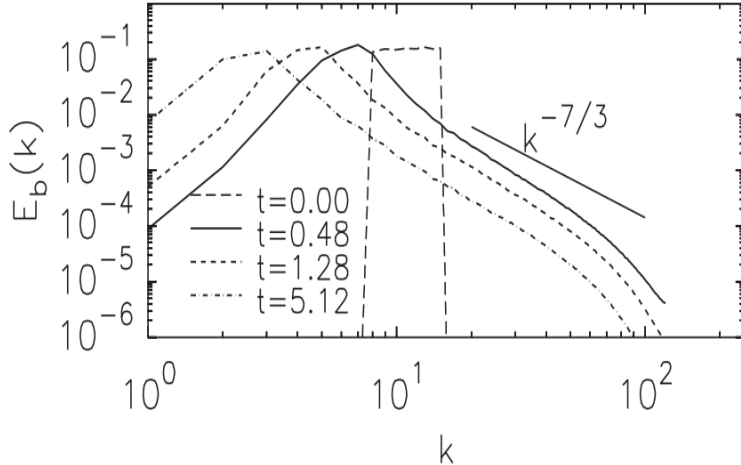


FIG. 17: Magnetic energy spectrum at different time. Reproduced with permission from [23].

Cho reported the study on the spectral evolution of helical electron magnetohydrodynamic (EMHD) waves and turbulence²³. EMHD is a fluid-like model for studies of waves and turbulence in space plasmas above and below the proton gyroscale. It is found that, unlike its MHD counterpart, an EMHD wave packet is dispersive. As a result, EMHD wave packets initially traveling in one direction create opposite-traveling wave packets via self-interaction and cascade energy to smaller scales. EMHD wave packets traveling in one direction clearly exhibit inverse energy cascade (Fig. 17), which is due to the conservation of magnetic helicity. Furthermore, as expected, it is evident that magnetic energy also exhibits forward cascade, with magnetic energy E_b spectrum following the power-law $E_b(k) \propto k^{-7/3}$. Here, k is wave number. Furthermore, the Kolmogorov spectrum and anisotropic structures during cascade of Alfvénic turbulence was numerically confirmed. The anisotropic dynamics suggests that smaller eddies are more elongated during the cascade²⁴.

IV. RECONNECTION AND PARTICLE ACCELERATION

Liu pursued the mechanism of fast magnetic reconnection rate of order 0.1. There is a long-standing puzzle about what is the underlying physics for the fast local magnetic reconnection rate $R_0 \sim 0.1$ in different systems²⁵. Here, R_0 is the normalized reconnection rate with respect to Alfvén velocity. Recently, a new simple model is developed to explain the possible physics mechanism for the fast magnetic reconnection. The key formula is given

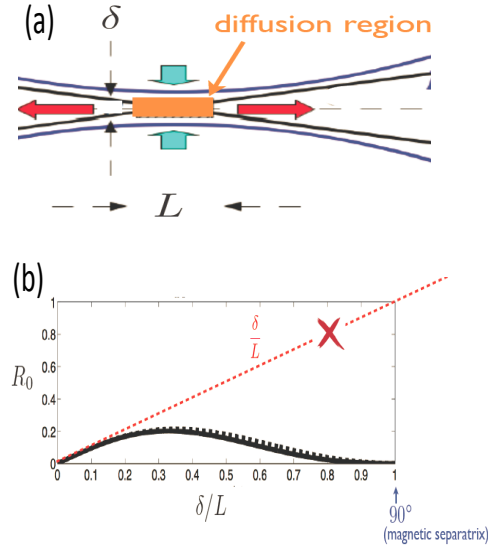


FIG. 18: (a) Sketch of magnetic field lines with the dimensions (δ and L) of the diffusion region. Here, δ and L are the thickness and length of diffusion region, respectively. (b) Reconnection rate R_0 as function of δ/L predicted by Eq.2. Dashed-red line is the result predicted by the Sweet-Parker model^{26–28}, which is invalid when the opening angle (i.e. δ/L) is relative large.

below.

$$R_0 \simeq \frac{\delta}{L} \left[\frac{1 - (\delta/L)^2}{1 + (\delta/L)^2} \right]^{-2} \sqrt{1 - (\delta/L)^2}. \quad (2)$$

It is suggested that the fast reconnection rate $R_0 \sim 0.1$ is a result of force-balance imposed on the inflow and outflow directions at the MHD scale (Fig. 18(a)), respectively. They are almost always applied in disparate systems, such as (i) PIC, hybrid, Hall-MHD, MHD simulations with a localized resistivity; (ii) both the non-relativistic and relativistic regimes; and (iii) asymmetric reconnection. Fig. 18(b) shows that the rate R_0 near its maximum is insensitive to δ/L (i.e. the opening angle of magnetic field separatrix). This potentially explains why reconnection has a similar fast rate for different models of the dissipation mechanism.

Hirota reported the progress on a theory for explosive reconnection based on the gyro-fluid energy principle framework²⁹. Two-fluid model including the Larmor radius effect is applied, in which the governing equations are the continuity and momentum equations for ions and electrons. The dispersion relation based on the energy principle is derived. When

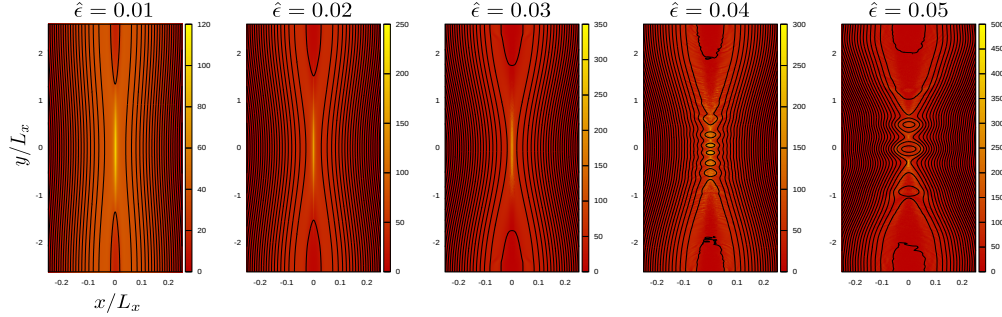


FIG. 19: Contours of magnetic field lines (solid line) and current distributions (color). Here, the perturbation $\hat{\epsilon}$ grows monotonically. The plasmoid instability is shown in right panels. Reprinted from [29], with permission from JSPF.

the energy principle based on gyro-fluid is applied to the tearing instability, it is found that: (i) only a two-parameter trial function for the inner layer (i.e. the current sheet layer) is enough to reproduce the analytical growth rate in various limits; (ii) the most unstable mode is easy to find. In addition, the skin depth of electron always destabilizes the tearing mode. For the case with finite plasma pressure, ions finite Larmor radius effect does not change the stability but always accelerates the growth rate. In the non-linear explosive phase, the reconnection speed is simply determined by the ideal-MHD energy balance in the external region (that is, in the whole region except for the current layer), and the most of magnetic energy is converted into the kinetic energy of the outflow. At the cold plasma limit, the plasmoid instability occurs instead of the production of a single X-shape current layer. In this case, the reconnection is intermittently accelerated in response to the plasmoid instability as shown in Fig.19, but never exceeds the explosive scaling³⁰. Plasmoid instability is fast enough to develop before the transition to the weak-nonlinear stage (i.e. Rutherford regime) of the magnetic reconnection.

Time scale of the reconnection is much shorter than the magnetic diffusion time scale induced by the resistivity. The collisionless effective resistivity may have a contribution to the fast connection rate. Ma proposed a physical model of effective resistivity for collisionless plasma³¹. Reconnection dynamics in MHD with inclusion of effective resistivity, $\eta_{eff} = \eta_e \frac{1}{1+(m_e T_e/m_i T_i)^{1/4}}$, is consistent with that from PIC simulation and MRX experiment. The effective resistivity may be used to explain characteristic length in space and laboratory plasmas. Here, η_e is the Spitzer resistivity. m_i and m_e are the electron and ion mass, respectively. T_i and T_e are the electron and ion temperature, respectively.

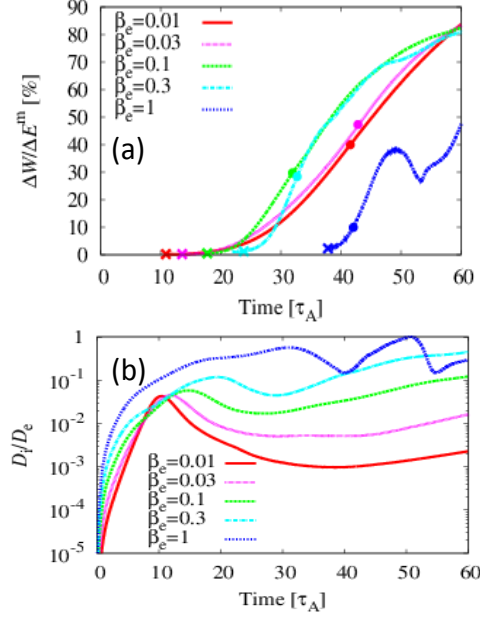


FIG. 20: (a) Dissipated energy (heating) over released magnetic energy against time (cross mark: peak of reconnection rate, dot mark: peak of electron-heating.); (b) ratio of ion dissipation to electron dissipation.

During magnetic reconnection, the magnetic field topology changes and the magnetic energy is explosively released, which is a candidate to explain why corona ($\sim 10^6$ K) is much hotter than photosphere (~ 6000 K). It is an essential problem to understand how the magnetic energy is converted to heat during magnetic reconnection. Numata pursued a numerical study of energy partition during the magnetic reconnection in weakly collisional plasmas. A gyro-kinetic simulation of magnetic reconnection was employed using the AstroGK code³². Here, finite, but small collisions are included and indispensable for the study of energy conversion process. It is found that phase mixing in both the parallel and perpendicular directions can be an important mechanism for plasma heating during the reconnection. Secondary plasmoid instability can change the reconnection rate and energy conversion process. Ion dissipation can be comparable to electron dissipation only for high-pressure, as shown in Fig. 20.

Tanabe reported the progress of the high field reconnection experiment on the MAST device. The energy conversion from magnetic field to particles are studied. It is found that (i) electron heating is highly localized around the X-point (Fig. 21(a)); (ii) ions are heated by outflow dissipation of plasma in the downstream (Fig. 21(b)); (iii) the larger toroidal

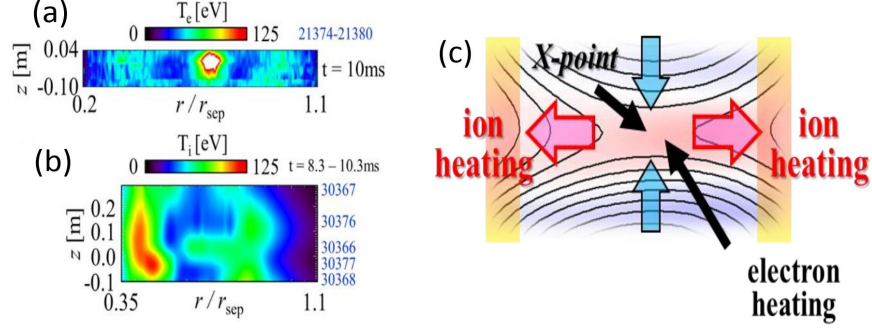


FIG. 21: Measurement of the electron (a) and ion temperature (b) during the magnetic reconnection. (c) Sketch of heating electrons and ions during reconnection. (a) and (b) are reproduced with permission from [33].

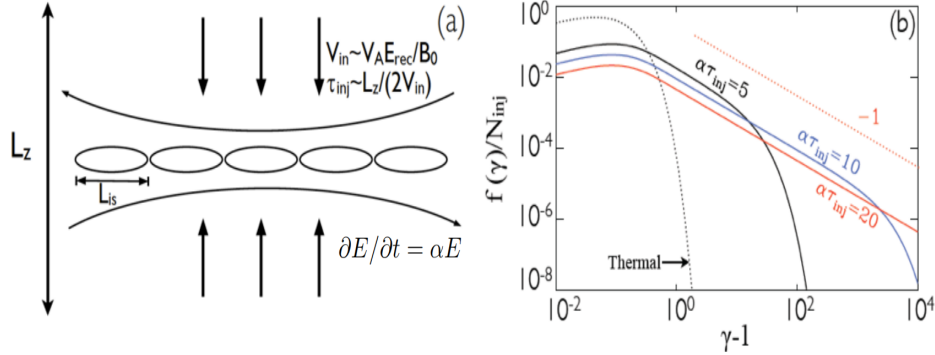


FIG. 22: (a) A model to explain the power-law energy spectrum predicted by PIC simulation for reconnection; (b) solution of energy-continuity equation for the energy ($E \propto \gamma - 1$) distribution function within the acceleration region for different acceleration rates α .

magnetic field produces the higher electron temperature around the X–point. While, magnetic field has negligible effect on the ion heating; (iv) the electron and ion temperatures form triple peaks during the relaxation phase^{33,34}.

F. Guo reported the results on the non-thermal particle acceleration in the magnetic reconnection, using the particle-in-cell (PIC) simulation technique. It is demonstrated that the reconnection layer is dominated by the development of flux ropes, and generates strong particle acceleration. For anti-parallel case, the acceleration is dominated by Femi-acceleration, and this leads to a robust energy distribution³⁵. When three-dimensional simulations are performed, a very turbulent reconnection layer is observed³⁶. Acceleration by parallel elec-

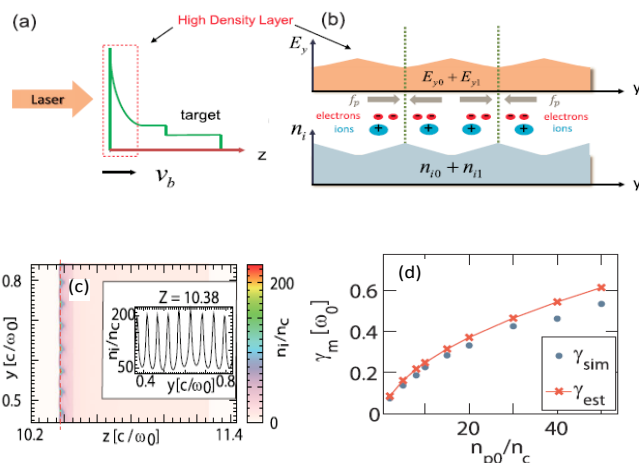


FIG. 23: (a) Schematic model of hole boring process by radiation pressure. (b) Physical picture of transverse instability within the high density layer. The z and y axes represent the longitudinal and transverse directions, respectively. The n_{i1} and E_{y1} represent the ion density and transverse electric field fluctuations, respectively. f_p represents the ponderomotive force. (c) Mode structure of transverse instability from 2D PIC simulation. (d) The predicted trend of wave number λ_m from theory agrees well with 2D PIC simulation. Reproduced with permission from [38].

tric field is important for reconnection with a strong guide field³⁷. In addition, a simple model was presented to explain the power-law energy spectrum observed in the PIC kinetic simulations^{35,36}. The model is illustrated by Fig. 22(a). As reconnection proceeds, cold plasma in the upstream region advects into the acceleration zone at a constant velocity that is determined by reconnection electric field. One can solve the energy-continuity equation for the energy distribution function $f(E, t)$ within the acceleration region. The solution is shown in Fig. 22(b) for several cases with $\alpha\tau_{inj} = 5, 10,$ and 20 . Here, α is the acceleration rate, and τ_{inj} is the time scale for the injection of particles from the upstream region.

In the field of particle acceleration, the transverse stability of the target is crucial for obtaining high quality ion beams, when the laser radiation pressure acceleration (RPA) technique is employed. However, the underlying physical mechanism is still a mystery. Wan showed that the coupling between transverse oscillating electrons and quasi-static ions can drive a transverse instability (Fig. 23)³⁸. The mechanism is similar to the oscillating two-stream-instability in the inertial confinement fusion research. The theoretically predicted

mode structure and growth rate agree well with the ones obtained from 2D PIC simulations in various regimes. The agreement suggests that the theory model contains essence of underlying physics of transverse breakup of the target. Here, the cold two-fluid model is applied in the theory analysis³⁸. In addition, a new scheme named the bi-color laser tweezer is proposed, which avoids the instabilities and shows good acceleration features (stable, monoenergetic, charges)

V. MHD AND ENERGETIC PARTICLE PHYSICS

Furukawa presented a new method for calculating magnetohydrodynamics (MHD) equilibrium, called simulated annealing (SA). SA is based on Hamiltonian formulation of dynamics of ideal fluids including ideal MHD. In the model, the system evolves on a surface specified by its energy and the Casimir invariants in the corresponding phase space. SA decreases the energy of the system monotonically, the obtained equilibrium has a lower energy compared to the initial condition. Therefore, if one starts the SA from a cylindrically symmetric state plus a tiny helical perturbation, the system goes to a helically deformed state if the cylindrically symmetric state is unstable, while the system comes back to the cylindrically symmetric state if it is stable. An example of such a helically deformed equilibrium can be found in Ref. 39.

Ma employed a dispersion relation (Eq. 3), based on the energy principle⁴⁰, to study the Beta-induced Alfvén Eigenmodes (BAE) and the energetic particle mode (EPM).

$$i\Lambda - \delta W_f - \delta W_k = 0. \quad (3)$$

Here, Λ , δW_f and δW_k represent the general inertial term, potential term and kinetic term associated with the particle non-adiabatic contribution.

Here, when $\delta W_f + Re(\delta W_k) < 0$ and the mode growth rate is determined by $Im(\delta W_k)$, the instability belongs to BAE variety. Whilst, when $\delta W_f + Re(\delta W_k)$ is close to zero and determines the mode real frequency, the corresponding instability (i.e. $Re(\Lambda^2) > 0$) is an EPM. It is found that the variation of magnetic shear results in the transition from BAE to EPM, which is again suppressed when magnetic shear is sufficiently large. Furthermore, finite orbit width of fast ion weakens the wave-particle resonance, thus resulting in decrease of BAE growth rate. When the non-perturbative wave-particle resonant effect is considered,

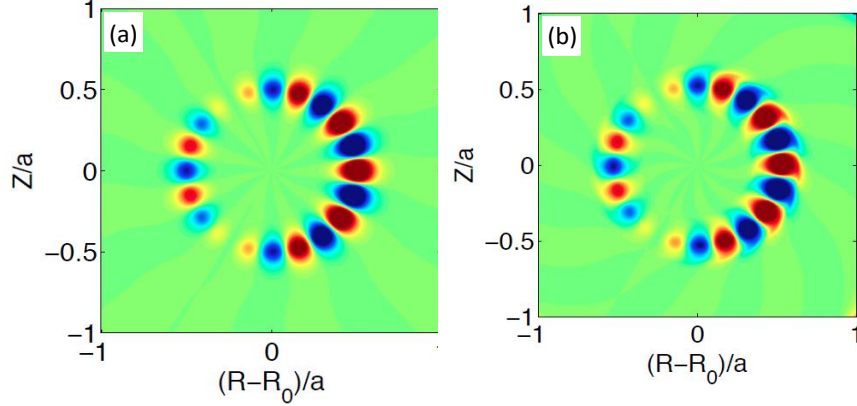


FIG. 24: Poloidal contour of the BAE structure without (a) and with (b) anti-Hermitian contribution.

the BAE is radially localized in the EP-pressure-gradient potential well and it is the most unstable in the lowest bound state. The anti-Hermitian contributions, due to wave-particle resonance, twist the radial mode structure, and lead to up-down asymmetry in the global mode structure⁴¹, as shown in Fig. 24. The results offer a theoretical explanation of existing experiments and numerical simulations which observe the asymmetric mode structure in the poloidal plane.

Song reported the results on the real-time control of neoclassical tearing mode (NTM) by the Electron Cyclotron Current Drive (ECCD) technique on the HL-2A device⁴². The instabilities are successfully suppressed by the ECCD system (Fig. 25), due to that the local current (driving source for TM) at the rational surface is significantly changed by the ECCD. The test of controlling Neoclassical-tearing-mode (NTM) will be carried out on the HL-2A device in the future.

Li reported the development of Bayesian SXR Tomography technique⁴³, which can potentially be applied to identify the spatial structure of MHD instabilities and to study the effect of MHD instabilities on impurity transport.

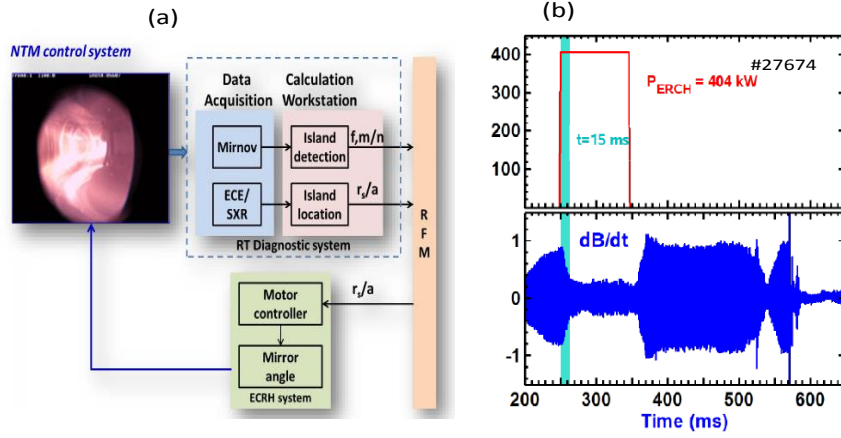


FIG. 25: (a) Sketch of the MHD control system on the HL-2A. (b) A representative case in which TM is stabilized when ECCD is turned on. (a) is reproduced with permission from [42].

VI. MAGNETIC CONFINEMENT PHYSICS FUNDAMENTALS

Ke investigated the energy transfer between drift-wave turbulence and shear flow. The kinetic energy equations for shear flow and turbulence can be expressed as

$$\frac{\partial}{\partial t} \frac{\langle u_j \rangle^2}{2} + \langle u_i \rangle \cdot \frac{\partial}{\partial x_i} \frac{\langle u_j \rangle^2}{2} = - \frac{\partial}{\partial x_i} (\langle \tilde{u}_j \tilde{u}_i \rangle \cdot \langle u_j \rangle) + \langle \tilde{u}_j \tilde{u}_i \rangle \frac{\partial}{\partial x_i} \langle u_j \rangle + \langle u_j \rangle \langle f_j^{ext} \rangle. \quad (4)$$

$$\frac{\partial}{\partial t} \frac{\langle \tilde{u}_j^2 \rangle}{2} + \langle u_i \rangle \cdot \frac{\partial}{\partial x_i} \frac{\langle \tilde{u}_j^2 \rangle}{2} = - \frac{\partial}{\partial x_i} \langle \frac{1}{2} \tilde{u}_j^2 \tilde{u}_i \rangle - \langle \tilde{u}_j \tilde{u}_i \rangle \frac{\partial}{\partial x_i} \langle u_j \rangle + \langle \tilde{u}_j \tilde{f}_j^{ext} \rangle. \quad (5)$$

Here, f_j^{ext} denotes the sum of all external forces, including pressure gradient, molecular viscosity, collision with electrons, etc. Einstein notation is applied here for brief expression. In tokamak edge plasma, considering the toroidal symmetry, $i, j = r, \theta$. To study the interaction between shear flow and turbulence, the Reynolds decomposition is applied as $u_j = \langle u_j \rangle + \tilde{u}_j$. Here, $\langle \cdot \rangle$ denotes average over time. Integrating Eq.(4) in a layer with width from r_1 to r_2 and considering $\langle u_r \rangle \sim 0$, u_θ is uniform in flux surface, one obtains

$$\frac{\partial}{\partial t} \int_{r_2}^{r_1} dr \frac{\langle u_\theta \rangle^2}{2} = - (\langle \tilde{u}_\theta \tilde{u}_r \rangle \cdot \langle u_\theta \rangle) |_{r_1}^{r_2} + \int_{r_1}^{r_2} dr \langle \tilde{u}_\theta \tilde{u}_r \rangle \frac{\partial}{\partial r} \langle u_\theta \rangle + \int_{r_1}^{r_2} dr \langle u_\theta \rangle \langle f_\theta^{ext} \rangle \quad (6)$$

It is shown that the first term on R.H.S of Eq.(4) represents the net shear flow energy change due to the interaction around the layer surface. This term is referred as surface effect. The

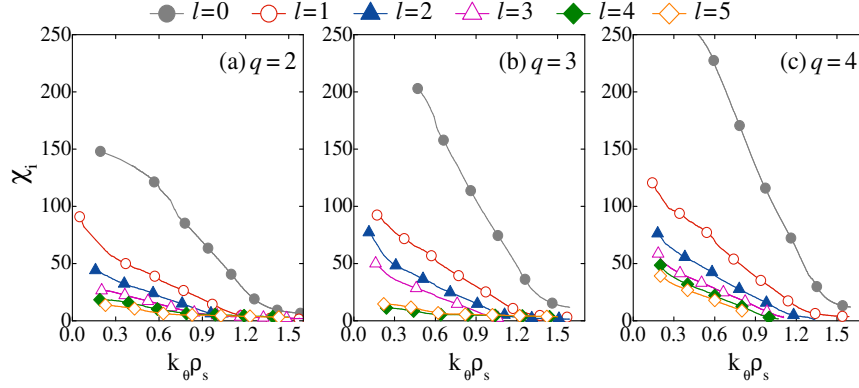


FIG. 26: Radial transport coefficient estimated with mixing length approximation for ITG modes with $l = 0-5$ versus $k_{\theta}\rho_s$. Here, ρ_s is the ion Larmor radius. (a), (b) and (c) are for different rational surfaces with $q = 2, 3, 4$, respectively. Reproduced with permission from [46].

second term on the R.H.S of Eqs.(4) and (5) represents energy transfer between turbulence and shear flow, and is referred to as the product of shear flow. It is found that the surface effect and turbulent spreading term are of the same order, and both of them are comparable with the production (energy transfer) term. It suggests that the surface effect and turbulent spreading should be included in the energy balance ⁴⁴.

Chen presented an analytical study on the nonlinear mode-mode coupling processes in toroidal geometry, by employing the nonlinear gyro-kinetic equations and ballooning-mode representation. It is found that the ballooning angle θ_k can change the structure of the drift-wave, and subsequently modify the linear stability properties and affect the overlapping between two normal modes⁴⁵. Meanwhile, θ_k also has the contribution to determine the direction of cascade of the collisionless trapped-electron-modes (CTEM) turbulence.

Han numerically studied the ion temperature gradient (ITG) modes in transport barriers (TBs) of tokamak plasma, using a gyrokinetic integral code. The full ion kinetic effects (the ion toroidal drift, transit motion, and finite Larmor radius) are included in the model. Multiple unconventional ITG mode structures ($l \neq 0$) are found in computations, in addition to the conventional instability with $l = 0$. Here, the mode-number l denotes a certain parity and the peak number of the mode eigenfunction in ballooning space. It is confirmed that both the ion temperature gradient and density gradient contribute to the drive of the unconventional ITG modes. In addition, the unconventional ITG mode is dominant

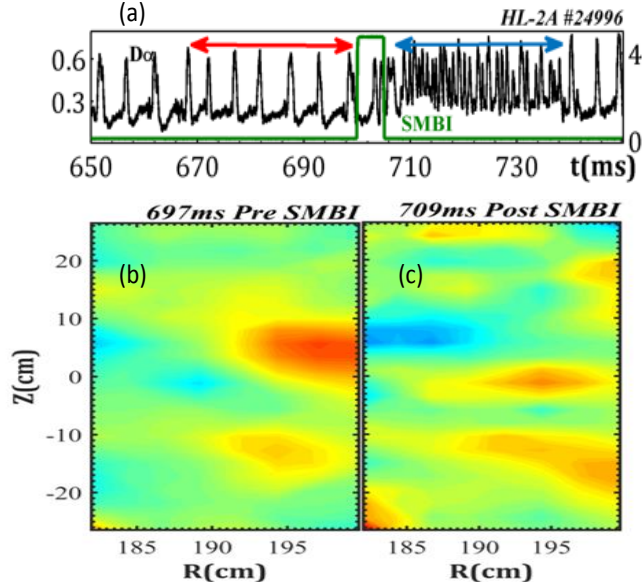


FIG. 27: (a) An example of ELM mitigation by SMBI on the HL-2A. (b) and (c) plot the ECE measured turbulence structure before and post of the ELM mitigation.

in both the small and large poloidal wave number ($k_{\theta}\rho_s$) regions, while the conventional one is dominant in the medium region of $k_{\theta}\rho_s$. Here, ρ_s is the ion Larmor radius. The transport coefficient induced by the unconventional modes is larger than that from the conventional one (Fig. 26)⁴⁶. The particle flux is outward and inward, when the ITG and trapped-electron-mode (TEM) are dominant, respectively.

Shi reported the results on the mitigation of edge-localized-modes (ELMs) by SMBI on the HL-2A⁴⁷ (Fig. 27(a)). SMBI leads to the increase of ELM frequency, and simultaneously the decrease of ELM amplitude. The mitigation effect is sensitive to the SMBI deposition position and injected particle intensity. When the deposition is in the outer part of the pedestal, mitigation is optimal. The Electron Cyclotron Emission (ECE) measurements indicate that, during ELM mitigation, turbulence structure is comparatively reduced as shown in Fig. 27(b) and (c). It implies that ELM mitigation is strongly correlated to the damping of the inward turbulence propagation in the pedestal. The underlying physics mechanism requires further theoretical and numerical investigations.

Yoo numerically investigated the particle transport in the Ohmic breakdown, using a particle simulation code BREAK (Breakdown Realistic Evolution Analysis in tokamaK). BREAK includes the following new physics for the breakdown: (i) the nature of gyro-motion

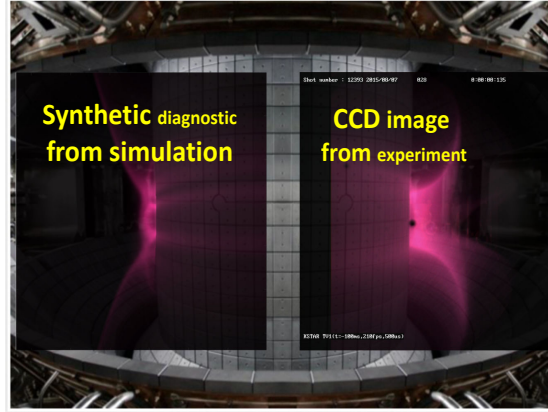


FIG. 28: Comparison of the simulated and measured emission structure during breakdown of the KSTAR discharge.

and guiding center motion and (ii) the roles of self-electric fields regarding strong magnetic fields. The critical role of self-electric fields on the breakdown process is confirmed, which has two important effects: (i) it strongly reduces the external electric field, and results in the significant decrease of the avalanche growth rate which leads to the relatively slow plasma formation; (ii) self-field induces the perpendicular anomalous transport, which is responsible for the homogeneous plasma structure along magnetic field lines. The simulation result from the BREAK code agrees well with experimental measurement as shown in Fig. 28.

Sugama extended the gyro-kinetic theory to include (i) general toroidal flow; (ii) temporal variation in both turbulent and background fields; (iii) appropriate collision model to keep the conservation of particles, energy, and momentum. The extended gyro-kinetic model is helpful for the long-term global transport simulation⁴⁸.

Liu reported the development of an accurate particle tracer (APT) code platform, which can be used to carry out long-term, large-scale particle simulations. In APT code, the full orbit model is employed. It is worth to point out that volume-preserving-algorithm is applied in computing, which guarantees the long-term numerical accuracy. One example of APT application is the long-term simulation of the runaway electron dynamics in tokamaks^{49,50}, with the time scale covering from the gyro-period ($\sim 10^{-11}$ s) to collision time (~ 0.5 s). The governing equations for describing runaway electron dynamics are presented below.

$$\frac{d\mathbf{x}}{dt} = \mathbf{v}, \quad (7)$$

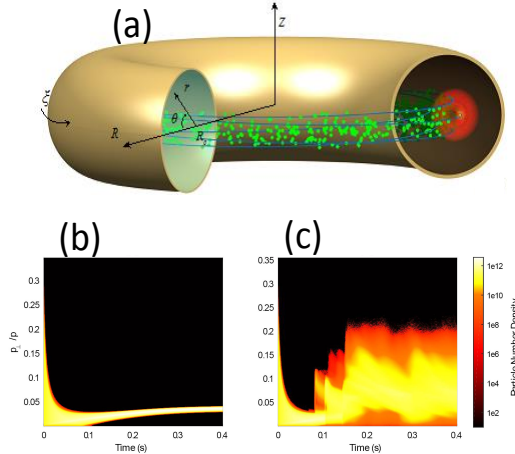


FIG. 29: (a) Sketch of the simulated configuration. Evolution of the pitch-angle distribution of the runaway electrons without (b) and with (c) the ripple magnetic fields.

$$\frac{d\mathbf{p}}{dt} = -e(\mathbf{E} + \mathbf{v} \times \mathbf{B}) + \mathbf{F}_R, \quad (8)$$

$$\frac{d\mathbf{x}}{dt} = \mathbf{v}. \quad (9)$$

Where \mathbf{x} , \mathbf{v} , and \mathbf{p} denote the position, velocity and relativistic momentum, respectively. \mathbf{F}_R is the electromagnetic radiation effect. It is found that due to the ripple field in the realistic configuration of tokamak, the collisionless pitch-angle scattering generates a broad spreading distribution of runaway electrons in the pitch-angle space (Fig. 29). In the ideal configuration, the mean energy value with a very small spread monotonically grows with time. Its trend is similar to the energy evolution of a single runaway electron in the ideal case. The APT is a well-designed integrated and modularized framework, which is universal and easily applied to other fields in physics.

VII. EXPLOITING FUNDAMENTALS FOR PERFORMANCE

Interaction between neutral gas and plasma is a fundamental problem which is studied in astrophysics, space plasmas, low temperature plasma, and nuclear fusion physics, etc. Wang reported the progress of module development for BOUT++ to study the interaction between neutral gas and plasmas and to study the associated particle transport^{51,52}. The newly developed modules are well validated with the HL-2A experiments associated with supersonic molecular beam injection (SMBI)⁵³. The predicted mean profiles of temperature/density,

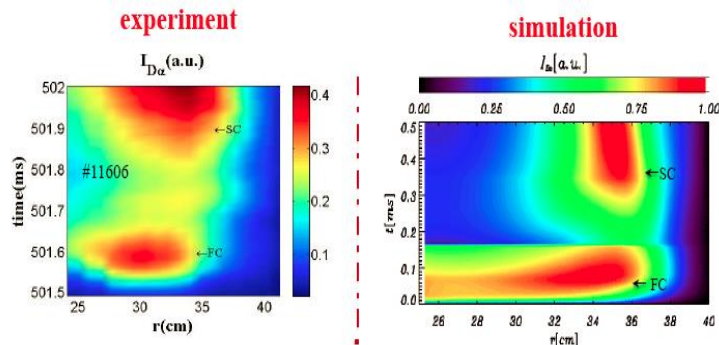


FIG. 30: Comparison of the measured(left) and simulated(right) fast and slow components(SC) during SMBI injection on the HL-2A.

fast/slow components (Fig. 30), and blocking effect during SMBI are consistent with the experimental measurements⁵³. Simulation of the neutral gas jet injection reveals that the fueling efficiency and penetration depth can be improved by adjusting injection fluxes and distances between plasmas and injector.

VIII. CONCLUSION

Fundamental plasma physics is important for reaching the goal of ITER, as designed⁵⁴. The studies of the basic plasma theory, self-organization, MHD instabilities, energetic particle physics, and plasma confinement contribute to the understanding of the pedestal dynamics, turbulent transport, access of improved plasma confinement and to the control of MHD and energetic particle instabilities in ITER. The operation of burning plasma in ITER will benefit from the progress of the fundamental plasma physics research. For example, the control of high performance plasma in ITER requires deep understanding of plasma response to the external sources, such as the resonant magnetic perturbation and impurity injection. In summary, the controlled fusion energy development requires the progress of the fundamental plasma physics.

Significant progress was achieved in many topics in fundamental plasma physics, as presented above, in the text of this paper. In dynamic sessions, with many stimulating presentations and intense discussions, many new ideas, results and suggestions are put forth. While there are many details of progress for the various topics, it is natural to ask: What is the

Topics		Questions
Basic plasma theory		What are the limitation of mean field (“quasi-linear”) theory? Can these be stated precisely?
Self-organization	(a) Flows	What is the branching ratio of energy between zonal structures and turbulence, especially for very low collisionality?
	(b) Magnetic	How do we understand and predict a state of incomplete Taylor relaxation?
Reconnection		Can the various “fast” reconnection scheme be unified from the perspective of electron momentum transport?
Magnetic confinement physics fundamentals		How optimize self-organized profile structure i.e. intrinsic rotation (residual stress), density peaking (pinch), etc, for giving heating mix? How does optimization work with RMP?
Exploiting fundamentals for performance		What is the optimal approach for ELM mitigation, i.e. SMBI, RMP, or QH operation? Or is I-mode a better option? Can we exploit our improving fundamental understanding to achieve a better practical result?

Table 2: Selected questions raised from the discussions during the meeting.

outcome? Here, we identify, without attribution, a specific question for each topical group, which emerges as the most interesting (Table 2). These questions will surely be the subjects of many discussions in future meetings. We look forward to hearing of progress on the above in Fundamental Sessions of future AAPPS-DPP meetings.

ACKNOWLEDGMENTS

Authors thank the all speakers who presented their work in the Fundamental Session of this conference, in particular, F.Guo, Z.B. Guo, M.K. Han, M. Hirota, R. Ke, Y.H. Liu., T. Long, R.R. Ma, Y. S. Na, R. Numata, Z.B. Shi, H. Tanabe, T.T. Tran, G. Vekstein, M. Veranda, L. Wang, M.G. Yoo, who provided highly valuable assistances in producing this summary report. We thank the referee for his thoughtful suggestions, leading to significant improvements in the manuscript. This work is supported by the U.S. Department of Energy, Office of Science, Office of Fusion Energy Sciences under Award Number DE-FG02-04ER54738. This is also supported by the Chinese National Natural Science Foundation under grant nos.U1867222 and 11775067

-
- ¹ Abstracts of 1st AAPPS-DPP, http://aappsdp.org/DPPPProgramlatest/topical_session.html.
- ² X. Fan, P. H. Diamond, L. Chacon, and H. Li, *Phys. Rev. Fluids* **1** (2016).
- ³ X. Fan, P. H. Diamond, and L. Chacon, *Phys. Rev. E* (2017).
- ⁴ D. Guo, L. Nie, R. Ke, M. Xu, Z. Wang, T. Long, Y. Wu, B. Yuan, S. Gong, H. Liu, and H.-A. Team, *Nucl. Fusion* **58**, 026015 (2018).
- ⁵ D. F. Escande, F. Doveil, and Y. Elskens, *Plasma Phys. Control. Fusion* **58**, 014040 (2016).
- ⁶ D. F. Escande, Y. Elskens, and F. Doveil, *Plasma Phys. Control. Fusion* **57**, 025017 (2015).
- ⁷ J. C. Hillesheim, J. C. Deboo, W. A. Peebles, T. A. Carter, G. Wang, T. L. Rhodes, L. Schmitz, G. R. Mckee, Z. Yan, and G. M. Staebler, *Phys. Rev. Lett.* **110**, 045003 (2013).
- ⁸ J.E. Rice, J.W. Hughes, P.H. Diamond, Y. Kosuga, Y.A. Podpaly, M.L. Reinke, M.J. Greenwald, O.D. Gurcan, T.S. Hahm, A.E. Hubbard, E.S. Marmor, C. J. McDevitt and D.G. Whyte, *Phys. Rev. Lett* **106**, 215001 (2011).
- ⁹ P.H. Diamond, Y. Liang, B.A. Carreras and P.W. Terry, *Phys. Rev. Lett* **72**, 2565 (1994).
- ¹⁰ R. Hong, G. Tynan, P. Diamond, L. Nie, D. Guo, T. Long, R. Ke, Y. Wu, B. Yuan, M. Xu, and The HL-2A Team, *Nucl. Fusion* **58**, 016041 (2018).
- ¹¹ S. C. Thakur, J. J. Gosselin, J. McKee, E. E. Scime, S. H. Sears, and G. R. Tynan, *Phys. Plasmas* **23**, 082112 (2016).
- ¹² M. J. Burin, G. R. Tynan, G. Y. Antar, N. A. Crocker, and C. Holland, *Phys. Plasmas* **12**, 84 (2005).
- ¹³ L. Cui, G. R. Tynan, P. H. Diamond, S. C. Thakur, and C. Brandt, *Phys. Plasmas* **22**, 511 (2015).
- ¹⁴ J. C. Li, P. H. Diamond, X. Q. Xu, and G. R. Tynan, *Phys. Plasmas* **23**, 056107 (2016).
- ¹⁵ S. Inagaki, T. Kobayashi, Y. Kosuga, S.-I. Itoh, T. Mitsuzono, Y. Nagashima, H. Arakawa, T. Yamada, Y. Miwa, N. Kasuya, M. Sasaki, M. Lesur, A. Fujisawa, K. Itoh, *Sci. Rep.* **6**, 22189 (2016).
- ¹⁶ L. Wang and P. H. Diamond, *Phys. Rev. Lett.* **110**, 265006 (2013).
- ¹⁷ S. Peng, L. Wang, and Y. Pan, *Nucl. Fusion* **57**, 036003 (2016).

- ¹⁸ T.T. Tran, S.S. Kim, H. Jhang, and J. Kim, *Plasma Phys. Control. Fusion*, in press (2019).
- ¹⁹ K. Zhao, Y. Nagashima, P. Diamond, J. Dong, K. Itoh, S.-I. Itoh, L. Yan, J. Cheng, A. Fujisawa, and S. Inagaki, *Phys. Rev. Lett* **117**, 145002 (2016).
- ²⁰ M. Veranda, D. Bonfiglio, S. Cappello, D. F. Escande, F. Auriemma, D. Borgogno, L. Chacon, A. Fassina, P. Franz, M. Gobbin, D. Grasso, and M. E. Puiatti, *Nucl. Fusion* **57**, 116029 (2017).
- ²¹ R.L. Dewar, Z. Yoshida, A. Bhattacharjee, and S. R. Hudson, *J. Plasma Phys.* **81**, 515810604 (2015).
- ²² R. L. Dewar, S. R. Hudson, A. Bhattacharjee, and Z. Yoshida, *Phys. Plasmas* **24**, 042507 (2017).
- ²³ J. Cho, *Phys. Rev. Lett.* **106**, 191104 (2011).
- ²⁴ J. Cho and A. Lazarian, *Astrophys. J.* **780**, 30 (2014).
- ²⁵ Y.-H. Liu, M. Hesse, F. Guo, W. Daughton, H. Li, P. A. Cassak, and M. A. Shay, *Phys. Rev. Lett.* **118**, 085101 (2017).
- ²⁶ P. A. Sweet, *IAU Symposium in Electromagnetic Phenomena in Cosmical Physics*, edited by B. Lehnert (Cambridge University Press, New York, 1958), p. 123. .
- ²⁷ E. Parker, *J. Geophys. Res.* **62**, 509 (1957).
- ²⁸ E. Parker, *Astrophys. J.* **8**, 177 (1963).
- ²⁹ M. Hirota, *Plasma Fusion Res.* **12**, 1401010 (2017).
- ³⁰ M. Ottaviani and F. Porcelli, *Phys. Rev. Lett* **71**, 3802 (1993).
- ³¹ Z.W. Ma, et.al., <http://aappsdp.org/DPPPprogramlatest/pdf/F-I26.pdf>.
- ³² R. Numata and N. F. Loureiro, *J. Plasma Phys.* **81**, 305810201 (2015).
- ³³ H. Tanabe, T. Yamada, T. Watanabe, K. Gi, K. Kadowaki, M. Inomoto, R. Imazawa, M. Gryaznevich, C. Michael, B. Crowley, N. J. Conway, R. Scannell, J. Harrison, I. Fitzgerald, A. Meakins, N. Hawkes, K. G. McClements, T. O’Gorman, C. Z. Cheng, and Y. Ono (The MAST Team), *Phys. Rev. Lett.* **115**, 215004 (2015).
- ³⁴ H. Tanabe, T. Yamada, T. Watanabe, K. Gi, M. Inomoto, R. Imazawa, M. Gryaznevich, R. Scannell, N. Conway, C. Michael, B. Crowley, I. Fitzgerald, A. Meakins, N. Hawkes, K. McClements, J. Harrison, T. O’Gorman, C. Cheng, Y. Ono, and T. M. Team, *Nucl. Fusion* **57**, 056037 (2017).
- ³⁵ F. Guo, H. Li, W. Daughton, and Y. H. Liu, *Phys. Rev. Lett.* **113**, 155005 (2014).
- ³⁶ F. Guo, Y.-H. Liu, W. Daughton, and H. Li, *Astrophys. J.* **806**, 167 (2015).

- ³⁷ X. Li, F. Guo, H. Li, and J. Birn, *Astrophys. J.* **855**, 80 (2018).
- ³⁸ Y. Wan, C.-H. Pai, C. J. Zhang, F. Li, Y. P. Wu, J. F. Hua, W. Lu, Y. Q. Gu, L. O. Silva, C. Joshi, and W. B. Mori, *Phys. Rev. Lett.* **117**, 234801 (2016).
- ³⁹ M. Furukawa and P. J. Morrison, *Plasma Phys. Control. Fusion* **59**, 054001 (2017).
- ⁴⁰ F. Zonca, L. Chen, and R. A. Santoro, *Plasma Phys. Control. Fusion* **38**, 2011 (1996).
- ⁴¹ R.R. Ma, et.al., <http://aappsdp.org/DPPPProgramlatest/pdf/F-O3.pdf>.
- ⁴² L. Yan, X. Ji, S. Song, F. Xia, Y. Xu, J. Ye, M. Jiang, W. Chen, T. Sun, S. Liang, F. Ling, R. Ma, M. Huang, H. Qu, X. Song, D. Yu, Z. Shi, Y. Liu, Q. Yang, M. Xu, X. Duan, and Y. Liu, *Rev. Sci. Instrum.* **88**, 113504 (2017).
- ⁴³ D. Li, Y. Liu, J. Svensson, Y. Liu, X. Song, L. Yu, R. Mao, B. Fu, W. Deng, B. Yuan, X. Ji, Y. Xu, W. Chen, Y. Zhou, Q. Yang, X. Duan, Y. Liu, and H.-A. Team, *Nucl. Fusion* **56**, 036012 (2016).
- ⁴⁴ R. Ke, et.al., <http://aappsdp.org/DPPPProgramlatest/pdf/F-I15.pdf>.
- ⁴⁵ H.T.Chen, et.al., <http://aappsdp.org/DPPPProgramlatest/pdf/F-O3.pdf>.
- ⁴⁶ M. Han, Z.-X. Wang, J. Dong, and H. Du, *Nucl. Fusion* **57**, 046019 (2017).
- ⁴⁷ Z. C. Yang, Z. B. Shi, W. L. Zhong, B. Y. Zhang, Q. C. Fan, H. D. Li, M. Jiang, P. W. Shi, C. Y. Chen, W. Chen, Z. T. Liu, D. L. Yu, Y. Zhou, B. B. Feng, X. M. Song, X. T. Ding, Q. W. Yang, X. R. Duan, and H.-A. Team, *Phys. Plasmas* **23**, 012515 (2016).
- ⁴⁸ H.Sugama, *Rev. Mod. Plasma Phys.* **1**, 9 (2018).
- ⁴⁹ J. Liu, Y. Wang, and H. Qin, *Nucl. Fusion* **56**, 064002 (2016).
- ⁵⁰ Y. Wang, H. Qin, and J. Liu, *Phys. Plasmas* **23**, 313 (2016).
- ⁵¹ Y. L. Zhou, Z. H. Wang, X. Q. Xu, H. D. Li, H. Feng, and W. G. Sun, *Phys. Plasmas* **22**, 012503 (2015).
- ⁵² Y. Shi, Z. Wang, Q. Ren, A. Sun, D. Yu, W. Guo, and M. Xu, *Chin. Phys. B* **26**, 55201 (2017).
- ⁵³ Z. H. Wang, X. Q. Xu, T. Y. Xia, and T. D. Rognlien, *Nucl. Fusion* **54**, 430 (2014).
- ⁵⁴ M. Shimada, D. Campbell, V. Mukhovatov, M. Fujiwara, N. Kirneva, K. Lackner, M. Nagami, V. Pustovitov, N. Uckan, J. Wesley, N. Asakura, A. Costley, A. Donn e, E. Doyle, A. Fasoli, C. Gormezano, Y. Gribov, O. Gruber, T. Hender, W. Houlberg, S. Ide, Y. Kamada, A. Leonard, B. Lipschultz, A. Loarte, K. Miyamoto, V. Mukhovatov, T. Osborne, A. Polevoi, and A. Sips, *Nucl. Fusion* **47**, S1 (2007).